[CANCER RESEARCH 62, 1890–1897, March 15, 2002]

Melanoma Tumors Acquire a New Phospholipid Metabolism Phenotype under Cystemustine As Revealed by High-Resolution Magic Angle Spinning Proton Nuclear Magnetic Resonance Spectroscopy of Intact Tumor Samples[1]

Daniel Morvan,[2] Aicha Demidem, Janine Papon, Monique De Latour, and Jean Claude Madelmont

Institut National de la Santé et de la Recherche Médicale U 484 [D. M., A. D., J. P., J. C. M.], and Centre de Lutte Contre le Cancer Jean Perrin, rue Montalembert [D. M., M. D. L.], 63005 Clermont-Ferrand, France

ABSTRACT

***N′*-[2-chloroethyl]-N[2-(methylsulfonyl) ethyl]-*N′*-nitrosourea (cystemustine), a chloroethylnitrosourea antineoplastic drug, provokes cellular proliferation inhibition and redifferentiation, but there was no cell death in B16 melanoma tumors. Because the phospholipid (Plp) metabolism is tightly involved in tumor growth regulation and tumor cell survival, we tested the hypothesis that melanoma tumors undergo adaptive Plp metabolism changes to survive treatment. Measurements of Plp derivatives were performed using a novel proton nuclear magnetic resonance Spectroscopy application using magic angle spinning on intact tumor tissue samples. Phosphatidylcholine levels were obtained from one-dimensional spectra, and relative levels of choline- and ethanolamine-containing compounds were derived from two-dimensional spectra (total correlation spectroscopy sequence). Two major findings emerged from this study: (*a*) during tumor growth inhibition, there was a transient accumulation of choline, glycerophosphocholine, and glycerophosphoethanolamine and a sustained increase in phosphocholine and phosphoethanolamine, whereas phosphatidylcholine levels remained unchanged; and (*b*) during tumor growth recovery, only phosphocholine and phosphoethanolamine remained elevated. Therefore, cystemustine-treated B16 melanoma tumors acquire a new Plp metabolism phenotype, a mechanism that could participate in tumor cell redifferentiation and/or survival.**

INTRODUCTION

CENU[3] are anticancer agents that mainly target DNA and create interstrand DNA bonds, thus interfering with tumor cell replication (1). We demonstrated previously that *N′*-[2-chloroethyl]-N[2-(methylsulfonyl)ethyl]-*N′*-nitrosourea (cystemustine), a CENU, provoked growth inhibition of B16 melanoma tumor with a drastic decrease in the number of mitoses, but there was no cell death (2). After a period of growth inhibition, tumor cells recovered a proliferation capability with the restoration of numerous mitoses, but the attained tumor mass remained much lower than that of untreated tumors over long-term follow-up (2). In addition, during the growth-inhibition period, tumor cells exhibited transient arrest in G_2 phase, redifferentiation features like increased tyrosinase activity and pigmentation, large cytoplasm, and loss of aggressiveness (2, 3). During growth recovery, redifferentiation features were still persistent.

Tumor growth regulation and cell survival tightly involves Plp metabolism (4–9). Apoptosis has been shown to be mediated by a drop in PtdCho mass because of an agent-induced blockage of the CDP-Cho pathway or to a mutation in CCT, the key enzyme of the CDP-pathway (5, 6). Cell growth has been shown to be inhibited, and even apoptosis induced, by alkyl-PC (10) or lysoPtdCho analogues (11). Additionally, the overexpression of PEMT, the enzyme converting PtdEth to PtdCho, inhibited hepatoma cell proliferation (7). Apoptosis could be prevented and cell differentiation induced through overexpression of PLC-γ (8). Moreover, water-soluble intermediates of Plp metabolism by themselves could play an important role in the regulation of mitogenesis and in cell survival (9). Among these derivatives, PC was shown to promote cell proliferation effects of insulin and insulin-like growth factor-1 (9).

In this study, we tested the hypothesis that cystemustine-TR murine B16 melanoma tumors undergo adaptive changes of Plp metabolism during the sequential phases of tumor evolution: the growth-inhibition period and the growth recovery period during which tumor cells proliferate again and exhibit a persistent redifferentiation pattern.

To this aim, we took advantage of ^{1}H-NMR Spectroscopy, a powerful tool to measure most Plp derivatives in intact cells and tissue or in extracts (4, 12). Because of improved signal:noise ratio techniques, two-dimensional NMR Spectroscopy now permits the identification and quantification of weakly concentrated species (13–15). A novel accessory, HRMAS when upgrading a high-field magnet, improves spectra of cell cultures (16), normal tissue (17, 18), and cancer tissue (19, 20). ^{1}H-HRMAS NMR Spectroscopy allowed us to simultaneously follow the fate of the Plp products and precursors, PtdCho, Cho, PC, CDP-Cho, Eth, PE, CDP-Eth, GPC, and GPE. Water-soluble Plp derivatives by themselves yield important information because their concentration plays a specific role in cell proliferation and survival (9), and they allow some Plp metabolism enzyme activities to be inferred (4).

The data presented in this report demonstrate, for the first time, that cystemustine-TR melanoma tumor cells maintain their PtdCho mass and acquire a new Plp derivative phenotype. During growth inhibition, tumors showed a transient increase in intracellular Cho, GPC, and GPE and a sustained increase in PC and PE, whereas PtdCho levels remained unchanged. During growth recovery, tumors overexpressed intracellular PC and PE, and the CDP-Eth pathway, a mechanism that could participate in B16 melanoma redifferentiation or protection against cell death.

MATERIALS AND METHODS

Chemical

N′-[2-chloroethyl]-N[2-(methylsulfonyl)ethyl]-*N′*-nitrosourea (cystemustine), a CENU antineoplastic agent (1), has been proposed in the treatment of human malignant melanoma and glioma. Cystemustine was used as a 5 mM solution in 0.9% NaCl. D_2O and $CDCl_3$ (SDS, Peypin, France) were used as solvents and as locking media for NMR Spectroscopy.

Received 6/8/01; accepted 1/16/02.

The costs of publication of this article were defrayed in part by the payment of page charges. This article must therefore be hereby marked *advertisement* in accordance with 18 U.S.C. Section 1734 solely to indicate this fact.

[1] Supported by: the Institut National de la Santé et de la Recherche Médicale (INSERM).

[2] To whom requests for reprints should be addressed, at INSERM U484, rue Montalembert, 63005 Clermont-Ferrand, France. Phone: +33 4 73 15 08 13; Fax: +33 4 73 15 08 01; E-mail: morvan@inserm484.u-clermont1.fr.

The abbreviations used are: CENU, chloroethylnitrosourea; Cho, choline; Eth, ethanolamine; PC, phosphocholine; PE, phosphoethanolamine; CDP-Cho, cytidine diphosphate choline; CDP-Eth, cytidine diphosphate ethanolamine; PtdCho, phosphatidylcholine; PtdEth, phosphatidylethanolamine; GPC, glycerophosphocholine; GPE, glycerophosphoethanolamine; PLA, phospholipase A; PLC, phospholipase C; Plp, phospholipid; CCT, CTP:phosphocholine cytidylyl transferase; PEMT, phosphatidylethanolamine *N*-methyl-transferase; NMR, nuclear magnetic resonance; HRMAS, high resolution magic angle spinning; HPF, high power field; TOCSY, total correlation spectroscopy; TR, treated; CPV, cross-peak volume; CT, control; Gly, Glycine; Lys, lysine.

Cell Cultures

Transplantable B16 melanoma cells originating from C57BL6/6J Ico mice were obtained from ICIG (Villejuif, France) and adapted to grow in culture. B16 cells were prepared as described previously (2).

Animal Model. Treatment Protocol

Six- to 8-week-old C57BL6/6J male mice were purchased from IFFA CREDO, (L'Arbresle, France). Mice were shaved before s.c. injections into their flank of 5×10^5 B16 cells. B16 melanoma tumors became palpable at days 7–9 after cell inoculation. Mice were divided into two groups, a CT group, which received sham injections of saline solution, and a TR group. The TR group received intratumor cystemustine injections at a dose of 15 μg/gram body weight. Cystemustine was injected at days 11, 14, and 18 from B16 cell inoculation.

At defined times of tumor evolution (days 10, 12, 15, 20, 24, and 29 after B16 cell inoculation for CT and TR tumors and prolonged to days 35, 43, and 54 for TR tumors), three mice of each group were sacrificed according to institutional guidelines for animal welfare and experimental conduct. Tumors were dissected and weighed. The dissection of the s.c. tumor took <2 min. A piece of the tumor <50 mg of the whole tumor was immediately prepared for NMR Spectroscopy as described below or frozen at −80°C in case of delayed examination.

Tumor growth curves were fitted to the Gompertz function and modified for the TR group to include a growth delay period. Ranges for maximum attainable weights and other model parameters obtained in cytomustine-treated melanoma models have been published previously (2).

Histopathology

Tumors underwent histopathological examination during follow-up. Formol-fixed tumors were embedded in paraffin, and 4-μm sections were cut for H&E staining analysis.

The count of mitoses was performed on 10 HPFs. Cell morphology and pigmentation load were evaluated.

Tissue Extracts

To further investigate the main Plp (PtdCho and PtdEth) content, chloroform/methanol tissue extracts were prepared from days 15–29 in CT and TR groups. Tissue samples were freeze dried and homogenized using a mortar and pestle. Then, 5 ml of chloroform/methanol (2:1, volume for volume) was added to the mixture, and the suspension was vortexed three times for 1 min and centrifuged at $1550 \times g$ for 5 min. The supernatant was collected and evaporated under dry nitrogen for 2 h. Extracts were reconstituted using $CDCl_3$, and 50 μl of extract were deposited in the dedicated NMR tube.

NMR Spectroscopy

NMR Spectroscopy was performed on a small bore Bruker DRX 500 magnet (Bruker, Karlsruhe, Germany) equipped with an HRMAS accessory. Samples were set into 4-mm diameter, 80-μl Zirconia rotor tubes. Three D_2O saline solution drops were added to the rotor tubes to lock the spectrometer, then rotors were spun at 4 kHz at room temperature.

The combination of a high-field magnet with the HRMAS accessory allowed us to obtain high resolution spectra of small amounts of material and minimized susceptibility artifacts because of air bubbles trapped inside the rotor, or to melanin content, a solid pigment that carries free radicals and retains paramagnetic metal ions like Fe^{3+}, and that may be strongly expressed in B16 melanoma cells.

Briefly, the HRMAS technique consists of spinning the sample at a rate <10 kHz about an axis tilted at an angle from the magnet axis. Sources of NMR line broadening in tissue include dipolar interaction in case the molecule has restricted mobility, anisotropy of molecular or tissue arrangement, and magnetic susceptibility effects because of the presence of paramagnetic material. These effects broaden NMR resonances by a factor of $D \times (3\cos^2(\theta) - 1)/2$, where D is the coupling constant (in Hz), and θ is the angle at which are oriented the molecular or the tissue internal axes or the paramagnetic center molecule of interest axis. If the tissue sample is rotated at a rate larger than D, broadening effects are averaged and, thus, reduced. Simultaneously setting θ at 54.7° (the magic angle) allows the chemical shift spreading to theoretically converge to zero. The HRMAS accessory then allows the use of the same radio-frequency power amplifiers and the same NMR sequences as the spectrometer standard equipment. In contrast, the technique differs from solid-state NMR Spectroscopy, which also uses magic angle spinning but operates at much higher rotation rates with dedicated NMR sequences and stronger radio-frequency power amplifiers.

NMR Spectroscopy of Intact Tumor Material

One-dimensional ^{1}H-NMR Spectroscopy. One-dimensional ^{1}H-NMR Spectroscopy of intact tumor material was used for the quantification of PtdCho. NMR Spectroscopy acquisition and processing were run from a workstation. After tuning and shimming from a shim table recorded previously, a water signal was obtained, and its frequency was retained for subsequent water signal suppression. An 8-μs radio-frequency pulse was applied, then 32 ^{1}H free induction decays were collected with water signal suppression at low power, a 10-ppm spectral width, 8 K complex data points, and a repetition time of 10 s. After Fourier transformation, a baseline correction was applied using a spline algorithm in the spectral domain of interest.

Peak referencing was done on the signal of 3-trimethylsilyl-propane sulfonate. PtdCho gave rise to a broad (because of restricted mobility) signal at 3.26 ppm (the trimethyl signal of the Cho moiety). However, the PtdCho signal overlapped with other signals at that spectral position and required the use of deconvolution procedures using the XWINNMR software (Bruker) to be quantified. Strong signals that could be separated from PtdCho were those of Taurine (Triplet at 3.27 ppm), PE (3.22 ppm), and the set of PC, CDP-Cho, and GPC (resonating together at 3.23 ppm). Signals of CDP-Eth, GPE, and PtdEth could not be resolved from that of PtdCho. However, they could be considered as negligible in comparison with PtdCho, because PtdCho was the most concentrated derivative among the four and because of its number of spins, the 3.26-ppm PtdCho signal weighed by 4.5-fold all Eth-containing derivative signals in the 3.2–3.3-ppm spectral area. Internal standardization was performed on the signal of Gly as discussed below in the two-dimensional NMR Spectroscopy section.

Two-dimensional ^{1}H-NMR Spectroscopy. The relative measurement of water-soluble Cho- and Eth-containing derivatives was performed on intact tumor material using a two-dimensional TOCSY sequence (13, 14). The sequence was performed with water signal suppression, using high-resolution sampling (spectral bandwidth of 6 ppm, 256 along the first axis, and 8 K complex data points along the second axis), a number of scans of 8, and a mixing time of 75 ms during which was applied a spin-lock pulse consisting of a cascade of short duration radio-frequency pulses aimed at producing a signal-enhancing polarization transfer effect. The repetition time was 2 s, thus weighting Plp derivatives by a factor of 0.98–0.92 (T_1s between 0.5 and 0.8 s) and the longest T_1 species (Gly, taurine) by a factor of 0.7 (T_1s of ~1.7 s). The phased mode was achieved using time proportional phase increment procedure. Raw data were processed with a quadratic sine function, then underwent Fourier transformation.

Proton resonances of the amine groups, Eth and Cho, are characteristic of each Plp derivative (given in ppm) and, because of scalar coupling, give rise to cross-correlation signals between hydrogen nuclei of neighbor CH_2 groups (the hyphen between chemical shifts indicates the scalar coupling): Cho (3.20 and 3.55–4.07), PC (3.23 and 3.62–4.18), CDP-Cho (3.23 and 3.68–4.39), GPC (3.23, 3.62, and 3.68–4.34), Eth (3.15–3.8), PE (3.22–3.99), CDP-Eth (3.30–4.20), and GPE (3.3–4.12).

The TOCSY sequence was optimized using a cascade of measurements on a mixture of Plp derivative standards, while varying only the mixing time. Optimal signal:noise ratio for most Plp derivatives was obtained for mixing times of 75 and 150 ms over a period of 200 ms (data not shown). We set our choice to 75 ms. The stability of the tissue sample inside the rotor was evaluated by a cascade of TOCSY measurements for ~10 h. We could verify that at room temperature, Plp derivatives varied by <20% after a 3-h stay inside the rotor. Operating with the sample cooled at temperatures <20°C would help improve the biological stability of the sample but at the expense of resolution (17). However, our overall sample processing and acquisition lasted by 105 min after excision, a duration which was short enough to adequately reflect Plp derivative changes that take place *in vivo*.

For quantification, real-part spectra were phased along both frequency axes

and baseline corrected using a low-order spline function. Then, CPVs were measured using the XWINNMR software from a recorded template of regions applied to the cross-peaks of interest (Cho, PC, GPC, CDP-Cho, Eth, PE, GPE, and CPD-Eth). CPVs were measured in the upper half plane of the spectrum where they were exempt from first-axis noise originating from strong signals like that of taurine at 3.27 ppm, also from partial saturation effects because of water signal suppression (21).

Two-dimensional spectra yield relative Plp derivative measurements, because CPVs are proportional to metabolite concentration, although weighted by relaxivity and magnetization transfer effects. T_1s of water soluble Plp derivatives were measured using Inversion Recovery-TOCSY (a sequence with TOCSY as the read block). Measured T_1s ranged between 500 and 800 ms. For each derivative, T_1s were similar in TR and CT groups (data not shown). In addition, Plp derivatives have similar spin systems. Therefore, cross-peak signal variations were mainly because of concentration variations. Internal standardization was performed using the diagonal signal of Gly at 3.56 ppm. The Lys ϵ-δ cross-peak signal has been proposed as an internal standard in two-dimensional NMR Spectroscopy, because it has been shown to be reasonably constant in a number of cell models and tissue samples (13). Lys ϵ-δ and Gly signals correlated in our study, irrespective of the sample group ($r^2 = 0.66$, $n = 42$). Normalization to the Lys ϵ-δ cross-peak signal or the Gly signal yielded similar time course curves (22). We chose to use the Gly signal here because the same standardization could be used in one- and two-dimensional spectra. Finally, standardizing the sample preparation, data acquisition and processing procedures ensured the comparability of spectra.

NMR Spectroscopy of Chloroform/Methanol Extracts

One-dimensional ^{1}H-NMR Spectroscopy. Relative quantification of PtdCho and PtdEth was performed using one-dimensional spectra of chloroform/methanol extracts, for which only these two Plp were quantifiable. Using the HRMAS coil did not greatly improve the resolution of extract spectra but did allow extracts to be reconstituted in high concentrations (microprobe), giving a signal advantage. Quantification was performed on the signals of PtdCho at 3.26 ppm and of PtdEth between 3.05 and 3.15 ppm corrected for their number of spins (nine and two, respectively). After baseline correction, Plp lines were fitted a mixed lorentzian-gaussian line using the XWINNMR software, then integrated, and the proportion of PtdCho and PtdEth relative to the sum of both was calculated.

Two-dimensional ^{1}H- NMR Spectroscopy. In extracts, TOCSY spectra were performed for PtdEth assignment. PtdCho gave rise to signals at 3.26 and 3.70 to 3.80–4.30 to 4.40 ppm and PtdEth at 3.05 to 3.15–4.00 to 4.15. The mixing time of the TOCSY sequence was set to 40 ms in accordance with published values for lipids (21).

Statistical Analysis

Data are presented as mean ± SD. Single comparisons between TR and CT groups were performed using the Mann-Whitney test. Time series were analyzed using ANOVA, followed by a post-hoc test with paired comparisons between TR and CT groups.

RESULTS

Cystemustine-TR B16 Melanoma Tumors Exhibit Transient Growth Inhibition and Sustained Redifferentiation. We compared tumor proliferation patterns in CT and cystemustine-TR groups by tumor size measurements, histopathology, and mitosis count. Tumor growth curves are shown in Fig. 1. In the CT group, measurements were only available until day 29 because the animals died. In the TR group, measurements were conducted until day 54. Two phases, accounted for by a Gompertz model, could be distinguished in CT tumors: (*a*) an exponential phase; and (*b*) a plateau phase starting from day 29 and characterized by the maximum attainable tumor weight. In the TR group, a growth-inhibition phase characterized by growth delay between days 12 and 24 was observed before a short exponential phase followed by a plateau phase characterized by tumor weights much lower than those of the CT tumors (1.1 ± 0.5 *versus* 5 ± 0.7 grams, $P < 0.001$, TR *versus* CT).

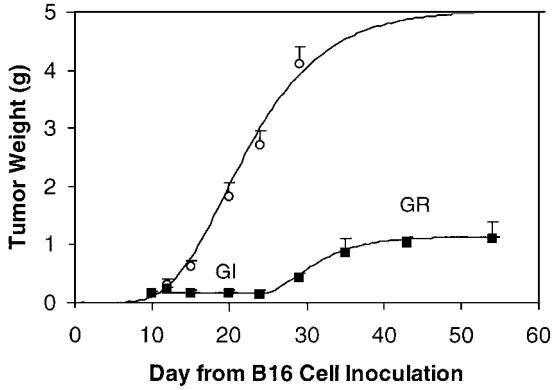

Fig. 1. Cystemustine-TR B16 melanoma tumors exhibit growth inhibition and growth recovery. Growth curves of CT (○) and cystemustine-TR (■) tumors with the best Gompertz fit superimposed. Cystemustine was administered intratumor between days 11 and 18. Each data point is the average of three experiments. *Bars*, SD. The CT curve showed an early exponential growth phase followed by a slowing down and a plateau phase. *GI*, growth inhibition; *GR*, growth recovery.

In CT tumors, histopathological examination revealed numerous mitoses, features of aggressiveness, and low-melanin content (Fig. 2*A*). In TR tumors, cells showed enlarged cytoplasm, features of decreased aggressiveness, and strong increase in melanin content (Fig. 2*B*). During the plateau phase, these redifferentiation features were still encountered, although they were weaker than during the growth-inhibition phase (Fig. 2*C*). This observation indicated that cystemustine induced a sustained redifferentiation pattern.

The count of mitoses per 10 HPF in the CT group was 104 ± 19 (days 12–29 average; Fig. 3). The mitosis count dropped at day 12 in the TR group. It averaged 7 ± 5 during the growth-inhibition phase (days 15–24), then increased and reached levels of 77 ± 29/10 HPF during the plateau phase, from days 35–54 ($P < 0.05$, TR *versus* CT at day 29).

During Growth Inhibition, Cystemustine-TR B16 Tumors Exhibit Transient Increase in Cho, GPC, and GPE and Sustained Elevation of PC and PE. Cho increased sharply at the beginning of the growth-inhibition phase and reached a maximum (2.2-fold the baseline level) at day 15, remained elevated until day 20, then decreased to CT levels (Fig. 4, *A* and *B* and Fig. 5*A*). PC increased from day 12 and reached a peak by 4.9-fold the pretreatment level at day 20, after the third cystemustine injection, then decreased moderately and was still elevated at day 29 (Fig. 4, *A* and *B* and Fig. 5*B*). After peaking, Cho could have fuelled the CDP-Cho pathway with PC (Fig. 5*B*) and CDP-Cho (data not shown) both culminating at day 20.

Eth levels did not vary during that period (data not shown). PE increased sharply during the growth-inhibition period and reached a maximum after the third cystemustine injection at day 20 by 3.6-fold, then decreased but remained elevated at day 29 (Fig. 4, *A* and *B* and Fig. 5*C*). The CDP-Eth level increased during the growth-inhibition phase and was still elevated at day 29 (Fig. 5*D*).

GPC and GPE increased during the growth-inhibition phase (Fig. 4, *A* and *B*). GPC and GPE culminated at day 20, after the third injection of cystemustine, by 2.8- and 2.7-fold, respectively, then decreased and reached the baseline at day 29 (Fig. 5, *E* and *F*).

During Growth Recovery, Cystemustine-TR B16 Tumors Exhibit Sustained Overexpression of PC and PE. Overall comparison of time course curves showed that PC and PE had parallel evolution, starting shortly after the first cystemustine administration.

During the plateau phase of TR tumors, Cho was low, whereas PC levels remained elevated 3-fold up to day 54 (Fig. 4*C* and Fig. 5*B*). CDP-Cho was lower than during growth inhibition.

In parallel, Eth levels did not vary, whereas PE levels remained

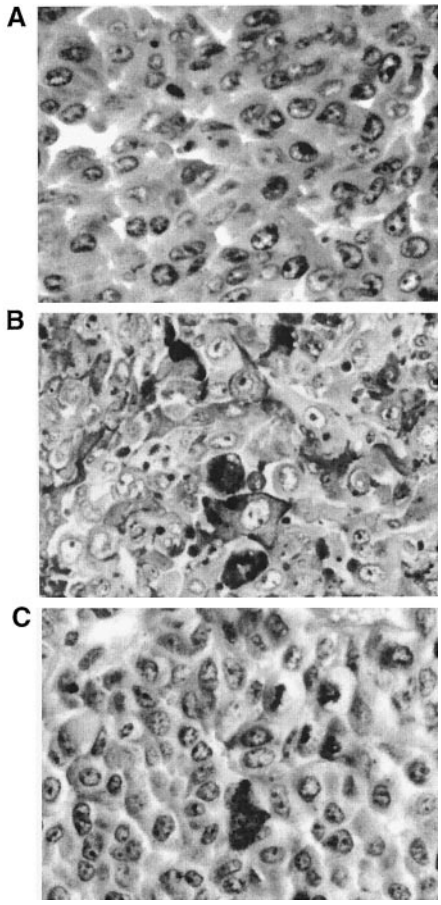

Fig. 2. In *A–C*, cystemustine-TR tumors exhibit histopathological features of decreased aggressiveness and redifferentiation. *A*, CT tumor at day 29. At the beginning of the plateau phase, the tumor showed important features of aggressiveness with many mitoses and a weak pigmentation load (×200). *B*, cystemustine-TR tumor at day 20. During the growth-inhibition phase, the tumor showed features of decreased aggressiveness, few mitoses, and an increased pigmentation content (×200). *C*, cystemustine-TR tumor at day 43. During the plateau phase, the count of mitoses was increased, but cells still displayed features of decreased aggressiveness and moderate pigmentation load (×200).

elevated 2.3-fold up to day 54 (Fig. 4*C* and Fig. 5*C*). CDP-Eth was increased with a sustained level until day 54 (Fig. 5*D*), indicating an involvement of the CDP-Eth pathway.

In contrast with other followed Plp derivatives that were transiently up-regulated during the growth-inhibition phase (Cho, GPC, and GPE; Fig. 5, *A*, *E*, and *F*), PC and PE were up-regulated over long-term evolution (Fig. 5, *B* and *C*), indicating the acquisition of a new Plp derivative phenotype by TR tumors during growth recovery.

Cystemustine-TR Tumors Maintain Plp Mass during Growth Inhibition and Recovery. PtdCho and PtdEth were the Plp the most highly expressed in melanoma tumors (Fig. 4*D*). The PtdCho curve displayed some oscillations in both groups (Fig. 6*A*). In the TR group, after day 12, PtdCho resumed its pretreatment levels for the duration of the growth-inhibition phase (until day 24), after which PtdCho reached a minimum at day 29, coinciding with the restoration of tumor growth. From that time on, the mitosis count increased (Fig. 3). Despite oscillations, the average PtdCho levels were similar in the TR and CT groups during the growth-inhibition phase (PtdCho/Gly time averaged over days 12–29: 2.8 ± 1.1 *versus* 2.7 ± 0.9, P = NS, TR *versus* CT) and also over complete evolution. In addition, the relative amounts of PtdCho and PtdEth measured from chloroform/methanol extracts and time averaged over days 15–29 were similar in TR and CT groups (Fig. 6*B*).

DISCUSSION

This study demonstrates the response of Plp metabolism to cystemustine, a DNA-damaging antineoplastic drug in a B16 melanoma murine model, during the sequential phases of TR tumor growth. Two major findings emerged from this study: (*a*) during growth inhibition, Cho, GPC, and GPE were transiently overexpressed, PC and PE showed sustained elevation, and PtdCho levels remained unchanged; and (*b*) during growth recovery, intracellular content of PC and PE remained elevated, indicating the acquisition of a new Plp derivative phenotype by regrowing cystemustine-TR tumors.

In this study, we provide simultaneous follow-up of most Cho- and Eth-containing Plp derivatives, including CDP-Cho and CDP-Eth, in intact tumors by ^{1}H-NMR Spectroscopy. Previous studies of Plp derivative expression have been carried out on cell cultures or tissue extracts (4, 12). The HRMAS technique has been shown to improve the detection of PtdCho in ^{1}H-NMR spectra of intact cells (16). We took advantage of HRMAS to quantify PtdCho levels in our study.

We focused on Plp derivatives rather than on enzyme activities. However, Plp derivatives allow some enzyme activities to be inferred and also have specific consequences when they accumulate (4, 9). PE was the most highly expressed Plp derivative in B16 melanoma. Similar findings were reported in other tumor models (4). Additionally, Ras transformation of NIH 3T3 fibroblast cells was shown to be associated with inhibition of CCT, activation of Cho- and Eth-kinase, and activation of PLC, yielding together an accumulation of PC and PE (23, 24). PC and PE accumulation in cancer cells is considered to play a role in the stimulation of mitogenesis (9).

The first major finding of this study was the profile of Plp derivatives during the growth-inhibition phase. Despite oscillations during follow-up, the average PtdCho levels were similar in the TR and CT groups. In the CT group, PtdCho levels were low during the early exponential growth phase possibly because of a strong membrane Plp demand that did not allow PtdCho to accumulate. PtdCho homeostasis is critical for cell survival. A recent study demonstrated that a mutant ovary cell line (MT58) exhibiting temperature-sensitive CCT activity underwent a G_1 cell cycle arrest, a drop in PtdCho level, and apoptosis at the critical temperature (5). Agents, such as nonmetabolizable analogues of lysoPtdCho, alkyl-PC, and tumor necrosis factor-α, were shown to induce a decrease in PtdCho mass or biosynthesis and provoke apoptosis (6, 10, 11). Alternatively, Plp accumulation inhibited cellular proliferation (25). In this study, the cystemustine-TR B16 tumors may have regulated their PtdCho mass to survive.

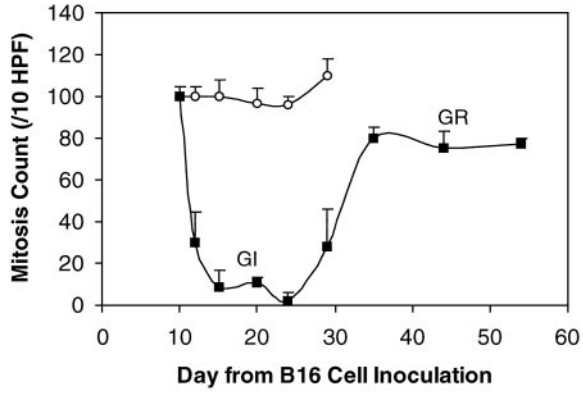

Fig. 3. Cystemustine-TR tumors exhibit changes in mitosis count during growth inhibition and recovery. The mitosis count in CT (○) and cystemustine-TR (■) tumors was performed on histopathological slices. Mitosis count dropped during the GI phase and then recovered to large values, although below CT ones, during the GR phase (77 ± 29 *versus* 104 ± 19 mitoses/10 HPF, $P < 0.05$, TR *versus* CT). *GI*, growth inhibition; *GR*, growth recovery.

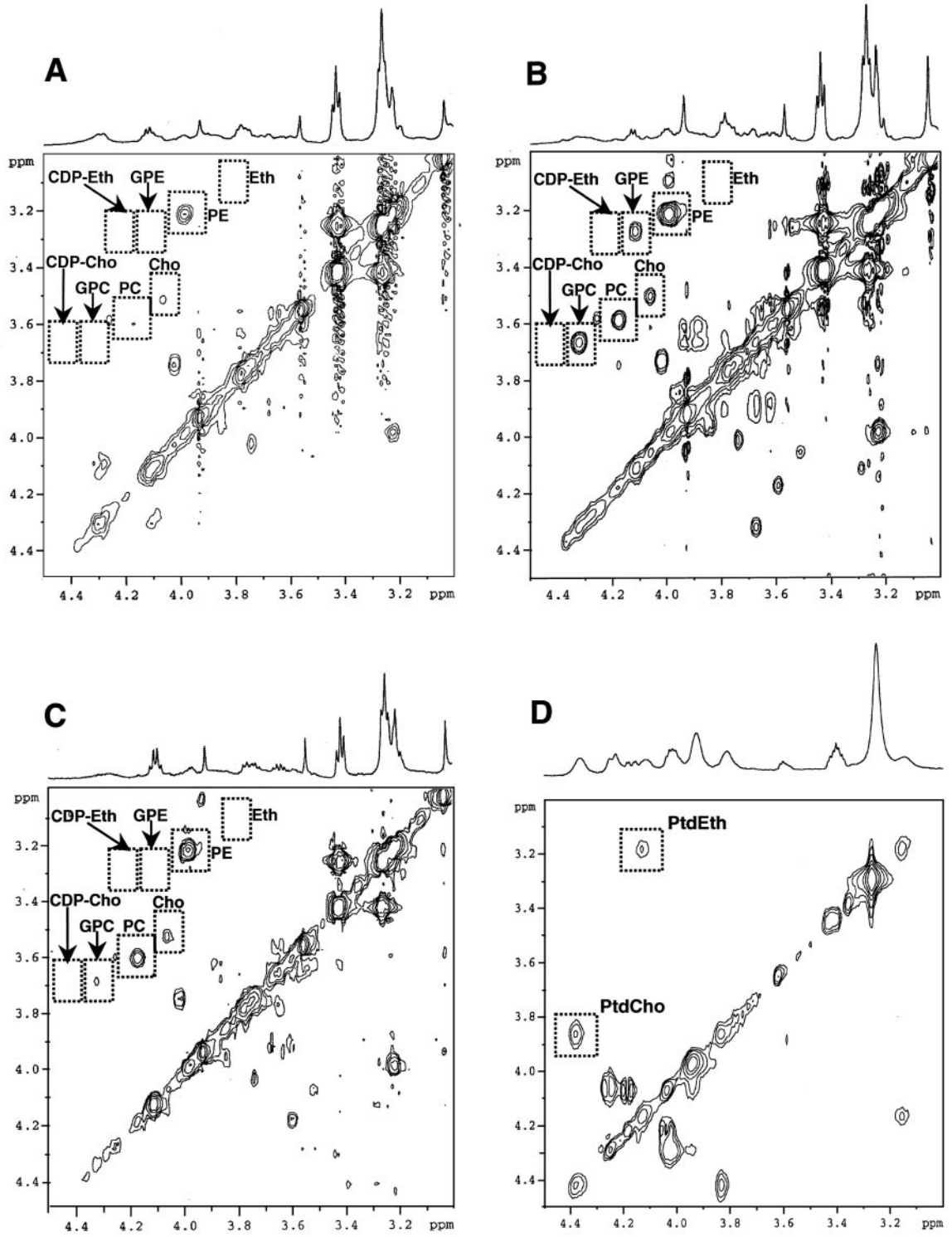

Fig. 4. *A–D,* typical one-dimensional and two-dimensional ^{1}H-NMR spectra in the 3–4.5-ppm spectral range. *A,* CT tumor at day 29 (beginning of the plateau phase). PE was the most highly expressed Plp derivative. *B,* cystemustine-TR tumor at day 20 (growth-inhibition phase). Cho, PC, PE, GPC, and GPE levels were increased in comparison with the CT tumor (*A*). *C,* TR tumor at day 43 (plateau phase). PE and PC levels were increased in comparison with the CT tumor (*A*). Cho, GPC, and GPE signals have returned to low levels in comparison with *B. D,* spectrum of chloroform extract of a CT tumor at day 29. PtdCho and PtdEth signals were easily identified. The number of isocontour lines indicates the higher content of PtdCho in comparison with PtdEth.

It has been shown that in response to Plp overload, *e.g.,* because of an excess in the culture medium, cells protect themselves through PLA2 activation and base-exchange activation (25). Cho may accumulate within the cells because of decreased release from the cells, increased production, or increased extracellular uptake. Because Cho increased at a time when PtdCho was in excess, Cho could originate from phospholipase D activation and/or base-exchange activation between PtdCho and PtdEth or phosphatidylserine (26). The catabolism of GPC into Cho and glycerol-phosphate is also a possible source of Cho through an activation of GPC-phosphodiesterase (27).

It appeared to be a likely involvement of the biosynthetic CDP-Cho pathway during days 20–29. This biosynthetic phase could have

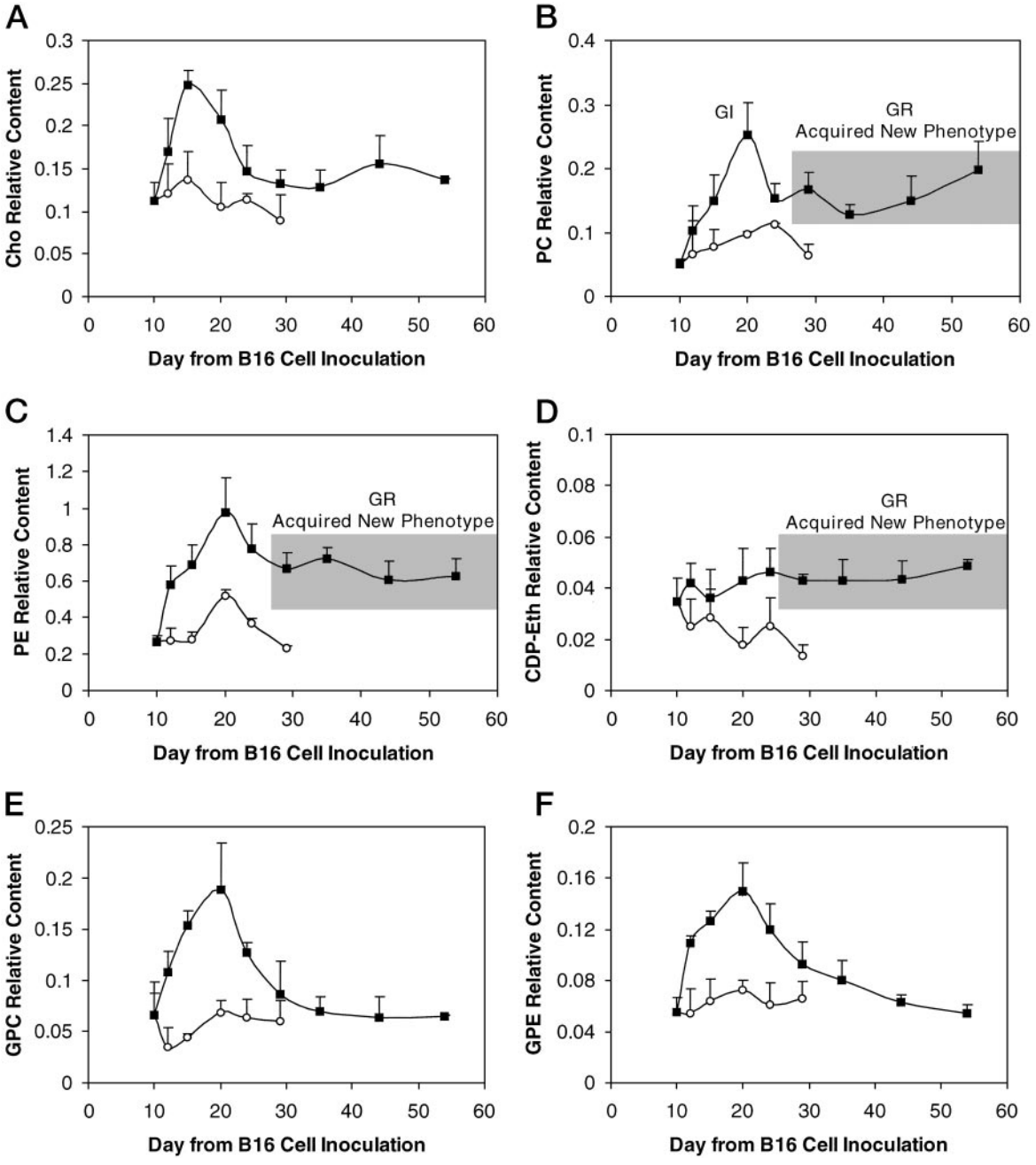

Fig. 5. In *A–E*, cystemustine-TR tumors show alterations in water-soluble derivatives during growth inhibition and recovery. Time course of Cho (*A*), PC (*B*), PE (*C*), CDP-Eth (*D*), GPC (*E*), and GPE (*F*) tissue relative content (see "Materials and Methods") in CT (○) and cystemustine-TR (■) tumors. Cystemustine was administered between days 11 and 18. Each data point was the average of three experiments. All variations were statistically significant (*Cho*: day-12 and day-15 data points, $P < 0.01$, TR *versus* CT; *PC*: day-15 data point and from days 24 to 54 data points, $P < 0.05$, day-20 data point, $P < 0.01$, TR *versus* CT (CT at day 29 for TR data points after day 29); *PE*: day-12 data point, $P < 0.05$, and from days 15 to 54 data points, $P < 0.01$; *CDP-Eth*: from day-20 data points, $P < 0.05$; *GPC*: day-12 and day-24 data points, $P < 0.05$, day-15 and day-20 data points, $P < 0.01$; *GPE*: day-12 and day-24 data points, $P < 0.05$, day-15 and day-20 data points, $P < 0.01$). *GI*, growth inhibition; *GR*, growth recovery.

prepared the tumor to recover growth. PtdCho is synthesized mainly via the CDP-Cho pathway and methylation of PtdEth involving PEMT (EC 2.1.1.71). In addition, differences between PtdCho profiles (acyl composition) occur according to the involved PtdCho biosynthesis pathway and should play a role in cellular proliferation processes (28, 29).

During growth inhibition, we observed a transient increase in GPC and GPE. These derivatives were released from PtdCho and PtdEth, respectively, through activation of PLA. GPC and GPE could accumulate because of a decrease in their turnover. The most likely hypothesis is that GPC and GPE accumulate because they are produced in excess through an activation of PLA2 (25). The quite elevated PtdCho levels observed during the growth-inhibition phase could be explained by a loss of demand for membrane Plp, thus allowing PtdCho to accumulate.

The involvement of PEMT under cystemustine treatment needs to be addressed. The PEMT pathway is quantitatively significant only in the liver (4). We showed previously in B16 melanoma that the methyl-transferase involved in creatine biosynthesis (EC 2.1.1.2) was activated during the growth-inhibition phase under cystemustine treatment (30). Recently, it has been reported that in Chinese hamster ovary-K1 cell cultures, the overexpression of PEMT did not inhibit

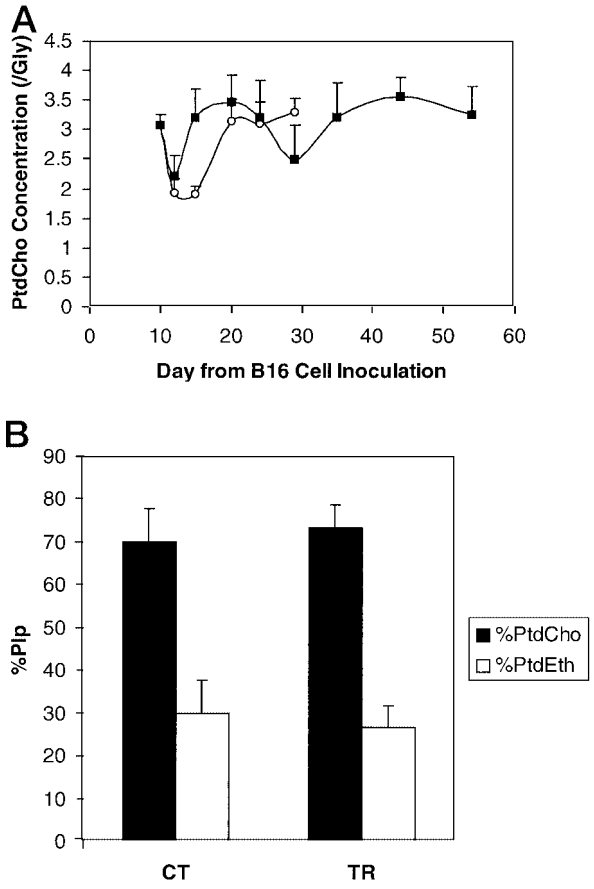

Fig. 6. In *A* and *B*, cystemustine-TR tumors maintain Plp mass during growth inhibition and recovery. *A*, time course of PtdCho:Gly ratio in CT (○) and cystemustine-TR (■) tumors. Each data point was the average of three experiments. There were no significant differences between TR and CT curves (ANOVA). *B*, relative ratios of PtdCho and PtdEth (each main Plp to the sum of both) obtained from one-dimensional ^{1}H-NMR spectra of chloroform/methanol extracts. Values were time averaged over days 15–29 (six measurements in each group; P = NS, TR *versus* CT).

the CDP-Cho pathway but paradoxically enhanced it (31). These data are to be compared with the report that the activation of PEMT produces a PtdCho functionally different from that derived from the CDP-Cho pathway (28, 29). Therefore, our data could be consistent with an activation of PEMT under cystemustine, a mechanism that would yield an excess PtdCho production with fatty-acid moieties of unusual types. It was shown that such activation inhibited cellular proliferation in hepatoma cells, and a similar process could account for tumor-growth inhibition in cystemustine-TR B16 melanoma.

The second major finding was that cystemustine-TR B16 tumor cells acquired a new Plp metabolism phenotype developed during the growth-inhibition phase, which became definitively acquired once tumors recovered growth. The new phenotype consisted of a sustained up-regulation of PC and PE under cystemustine treatment. PC and PE alterations have been reported in a number of tumor cells and tissues (4), but their relation with active cell proliferation or other mechanisms remains unclear. PC and PE increases in our study probably resulted from sequential activation of Cho- and Eth-kinase and/or of PLC (23, 24). However, to date, mammalian PLC activity hydrolyzing PtdEth has not been demonstrated (4, 32). In addition, during tumor-growth recovery, Cho and Eth were quite low, consistent with an up-regulation of Cho- and Eth-kinases. Therefore, our favored explanation was an activation of Cho- and Eth-kinases to explain the phenotype change during growth recovery. Thus, cells, rather than die, would modify their phenotype through a sustained Cho- and Eth-kinase activation. However, not only enzyme activation, but also substrate accumulation, should play a role in cell proliferation. PC in itself promotes mitogenesis through an increased rate of PtdCho synthesis and sensitization to mitogenic factors like insulin and insulin-like growth factor-1 (9).

We also found an involvement of the CDP-Eth pathway. It accompanied the increased PE level and could account for an activation of PEMT or the Eth cycle, two processes related to the mitogenic potential (28, 29, 32).

TR tumors acquired another Plp metabolism phenotype, most likely the consequence of an increased expression or activation of Cho- and Eth-kinases or one of their isoforms (9). Some studies have demonstrated that gene expression may be modified because of CENU treatment (33–35). CENU induced mitogen-activated protein kinase genes (33) and decreased the expression of DNA-repair genes (33, 35), involving a methylation of the gene promoter in nonresistant tumors (34).

In conclusion, this study demonstrates that cystemustine-TR B16 melanoma tumors develop adaptive Plp metabolism changes *in vivo*. During the growth-inhibition phase, TR tumors transiently overexpressed Cho, GPC, and GPE, whereas they maintained Plp mass at CT values. Over long-term evolution (during growth inhibition and subsequent recovery), TR tumors overexpressed PC and PE, indicating the acquisition of a new phenotype, a mechanism that could be associated with tumor cell redifferentiation and/or survival.

REFERENCES

1. Godeneche, D., Rapp, M., Thierry, A., Laval, F., Madelmont, J. C., Chollet, P., and Veyre, A. DNA damage induced by a new 2-chloroethyl nitrosourea on malignant melanoma cells. Cancer Res., *50:* 5898–5903, 1990.
2. Demidem, A., Morvan, D., Papon, J., De Latour, M., and Madelmont, J. C. Cystemustine induces redifferentiation of primary tumors and confers protection against secondary tumor growth in a melanoma murine model. Cancer Res., *61:* 2294–2300, 2001.
3. Buchdahl, C., Papon, J., Communal, Y., Bourges, M., and Madelmont, J. C. G2 accumulation and melanin overproduction in malignant melanocytes treated with a new nitrosourea. Melanoma Res., *8:* 517–527, 1998.
4. Podo, F. Tumor phospholipid metabolism. NMR Biomed., *12:* 413–439, 1999.
5. Cui, Z., Houweling, M., Chen, M. H., Record, M., Chap, H., Vance, D. E., and Tercé, F. A genetic defect in phosphatidylcholine biosynthesis triggers apoptosis in Chinese Hamster Ovary cells. J. Biol. Chem., *271:* 14668–14671, 1996.
6. Mallampalli, R. K., Ryan, A. J., Salome, R. G., and Jackowski, S. Tumor necrosis factor-α inhibits expression of CTP:phosphocholine cytidylyltransferase. J. Biol. Chem., *275:* 9699–9708, 2000.
7. Cui, Z., Houweling, M., and Vance, D. E. Expression of phosphatidylethanolamine *N*-methyltransferase-2 in McArdle-RH7777 hepatoma cells inhibits the CDP-choline pathway for phosphatidylcholine biosynthesis via decreased gene expression of CTP:phosphocholine cytidylyltransferase. Biochem. J., *312:* 939–945, 1995.
8. Lee, Y. H., Kim, S., Kim, J., Young Kim, K., Kim, M. J., Ryu, S. H., and Suh, P. Overexpression of phospholipase C-γ1 suppresses UVC-induced apoptosis through inhibition of c-fos accumulation and c-Jun *N*-terminal kinase activation in PC12 cells. Biochim. Biophys. Acta, *1440:* 235–243, 1999.
9. Kiss, Z. Regulation of mitogenesis by water-soluble phospholipid intermediates. Cell Signal., *11:* 149–157, 1999.
10. Wieder, T., Orfanos, C. E., and Geilen, C. Induction of ceramide-mediated apoptosis by the anticancer phospholipid analog, hexadecylphosphocholine. J. Biol. Chem., *273:* 11025–11031, 1997.
11. Baburina, I., and Jackowski, S. Apoptosis triggered by 1-*O*-Octadecyl 2-*O*-methyl-rac-glycero-3-phosphocholine is prevented by increased expression of CTP-Phosphocholine Cytidylyltransferase. J. Biol. Chem., *273:* 2169–2173, 1998.
12. Ackerstaff, E., Pflug, B. R., Nelson, J. B., and Bhujwalla, Z. M. Detection of increased choline compounds with proton nuclear magnetic resonance spectroscopy subsequent to malignant transformation of human prostatic epithelial cells. Cancer Res., *61:* 3599–3603, 2001.
13. Sivaraja, M., Turner, C., Souza, K., and Singer, S. *Ex-vivo* two-dimensional proton nuclear magnetic resonance spectroscopy of smooth muscle tumors: advantages of total correlated spectroscopy over homonuclear J-correlated spectroscopy. Cancer Res., *54:* 6037–6040, 1994.
14. Delikatny, E. J., Roman, S. K., Hancock, R., Jeitner, T. M., Lander, C. M., Rideout, D. C., and Moutford, C. E. Tetraphenylphosphonium chloride induced NMR visible lipid accumulation in a malignant human breast cell line. Int. J. Cancer, *67:* 72–79, 1996.
15. Moreno, A., Lopez, L. A., Fabra, A., and Arus, C. ^{1}H MRS markers of tumor growth in intrasplenic tumors and liver metastasis induced by injection of HT-29 cells in nude mice spleen. NMR Biomed., *11:* 93–106, 1998.

16. Weibright, P., Millis, K., Campbell, N., Cory, D. G., and Singer, S. Gradient high resolution magic angle spinning ^{1}H nuclear magnetic resonance spectroscopy of intact cells. Magn. Reson. Med., *39:* 337–344, 1998.
17. Middleton, D. A., Bradley, P. D., Connor, S. C., Mullins, P. G., and Reid, D. G. The effect of sample freezing on proton magic-angle spinning NMR spectra of biological tissue. Magn. Reson. Med., *40:* 166–169, 1998.
18. Garrod, S., Humpfer, E., Spraul, M., Connor, S. C., Polley, S., Connelly, J., Lindon, J. C., Nicholson, J. K., and Holmes, E. High resolution magic angle spinning ^{1}H-NMR spectroscopic studies on intact rat renal cortex and medulla. Magn. Reson. Med., *41:* 1108–1118, 1999.
19. Cheng, L. L., Lean, C. L., Bogdanova, A., Wright, S. C., Ackerman, J. L., Brady, T. J., and Garrido, L. Enhanced resolution of proton NMR spectra of malignant lymph nodes using magic angle spinning. Magn. Reson. Med., *36:* 653–658, 1996.
20. Moka, D., Vorreuther, R., Schicha, H., Spraul, M., Humpfer, E., Lipinski, M., Foxall, P. J. D., Nicholson, J. K., and Lindon, J. C. Biochemical classification of kidney carcinoma biopsy samples using magic-angle-spinning ^{1}H nuclear magnetic resonance spectroscopy. J. Pharm. Biomed. Anal., *17:* 125–132, 1998.
21. Gillet, B., and Doan, B. T. Phase sensitive two-dimensional experiment on living animals. J. Magn. Reson. Series B, *108:* 44–49, 1995.
22. Morvan, D., Demidem, A., Papon, J., and Madelmont, J. C. Imbalance of CDP pathways and up-regulation of phosphoethanolamine under CENU treatment in long term cultures of malignant melanoma cells. A ^{1}H-HRMAS study. Proc. Intl. Soc. Magn. Reson. Med., *9:* 2229, 2001.
23. Momchilova, A., and Markovska, T. Phosphatidylethanolamine and phosphatidylcholine are sources of diacylglycerol in *ras*-transformed NIH 3T3 fibroblasts. (1999) Int. J. Biochem. Cell Biol., *31:* 311–318, 1999.
24. Momchilova, A., Markovska, T., and Pankov, R. Ha-*ras*-transformation alters the metabolism of phosphatidylethanolamine and phosphatidylcholine in NIH 3T3 fibroblasts. Cell Biol. Int., *23:* 603–610, 1999.
25. Baburina, I., and Jackowski, S. Cellular responses to excess phospholipid. J. Biol. Chem., *274:* 9400–9408, 1999.
26. Stone, S. J., and Vance, J. E. Cloning and expression of murine liver phosphatidylserine synthase PSS-2: differential regulation of phospholipid metabolism by PSS1 and PSS2. Biochem. J., *342:* 57–64, 1999.
27. Belardelli, F., Proietti, E., Ciolli, V., Sestili, P., Carpinelli, G., Di Vito, M., Ferretti, A., Woodrow, D., Boraschi, D., and Podo, F. Interleukin-1 β induces tumor necrosis and early morphologic and metabolic changes in transplantable mouse tumors. Similarities with the anti-tumor effects of tumor necrosis factor α or β. Int. J. Cancer, *44:* 116–123, 1989.
28. Delong, C. J., Shen, X. J., Thomas, M. J., and Cui, Z. Molecular distinction of phosphatidylcholine synthesis between the CDP-Choline pathway and phosphatidylethanolamine methylation pathway. J. Biol. Chem., *274:* 29683–29688, 1999.
29. Waite, K. A., and Vance, D. E. Why expression of phosphatidylethanolamine N-methyltransferase does not rescue Chinese hamster ovary cells that have an impaired CDP-choline pathway. J. Biol. Chem., *275:* 21197–21202, 2000.
30. Demidem, A., Morvan, D., Papon, J., and Madelmont, J. C. Cystemustine treatment shifts methionine metabolism towards creatine production during growth arrest in a murine melanoma model. Proc. Am. Assoc. Cancer Res., *42:* 203, 2001.
31. Lee, M. K., Bakovic, M., and Vance, D. E. Overexpression of phosphatidylethanolamine *N*-methyl transferase-2 in CHO K1 cells does not attenuate the activity of the CDP choline pathway for phosphatidylcholine biosynthesis. Biochem. J., *320:* 905–910, 1996.
32. Shiao, Y. J., and Vance, J. E. Evidence for an ethanolamine cycle: differential recycling of the ethanolamine moiety of phosphatidylethanolamine derived from phosphatidylserine and ethanolamine Biochem. J., *310:* 673–679, 1995.
33. Rhee, C. H., Ruan, S., Chen, S., Chenchik, A., Levin, V. A., Yung, A. W., Fuller, G. N., and Zhang, W. Characterization of cellular pathways involved in glioblastoma response to the chemotherapeutic agent 1,3-bis (2-chloroethyl)-1-nitrosourea (BCNU) by gene expression profiling. Oncol. Rep., *6:* 393–401, 1999.
34. Esteller, M., Garcias-Foncillas, J., Andion, E., Goodman, S. N., Hidalgo, O. F., Vanaclocha, V., Baylin, S. B., and Herman, J. G. Inactivation of the DNA-repair gene *MGMT* and the clinical response of gliomas to alkylating agents. N. Engl. J. Med., *343:* 1350–1354, 2000.
35. Cai, Y., Wu, M. H., Xu-Welliver, M., Pegg, A. E., Ludeman, S. M., and Dolan, M. E. Effects of *O*6-benzylguanine on alkylating agent-induced toxicity and mutagenicity in CHO cells expressing wild-type and mutant O6-alkylguanine-DNA alkyltransferases. Cancer Res., *60:* 5464–5469, 2000.

Melanoma Tumors Acquire a New Phospholipid Metabolism Phenotype under Cystemustine As Revealed by High-Resolution Magic Angle Spinning Proton Nuclear Magnetic Resonance Spectroscopy of Intact Tumor Samples

Daniel Morvan, Aicha Demidem, Janine Papon, et al.

Cancer Res 2002;62:1890-1897.